ELSEVIER

Journal of Structural Geology 27 (2005) 1954–1972

JOURNAL OF STRUCTURAL GEOLOGY

www.elsevier.com/locate/jsg

Influence of mechanical stratigraphy and initial stress state on the formation of two fault propagation folds

Néstor Cardozo[a,*], Richard W. Allmendinger[b], Julia K. Morgan[c]

[a]*Center for Integrated Petroleum Research, Allegaten 41, N-5007 Bergen, Norway*
[b]*EAS Department, Cornell University, Ithaca, NY 14853, USA*
[c]*Department of Earth Science, Rice University, Houston, TX, USA*

Received 12 October 2004; received in revised form 8 June 2005; accepted 8 June 2005
Available online 9 August 2005

Abstract

Kinematic and mechanical modeling of the Rip Van Winkle (SE New York, USA) and La Zeta (SW Mendoza, Argentina) anticlines illustrate the influence of mechanical stratigraphy and initial stress state on the kinematics of fault propagation folding. In both anticlines, faults nucleating at distinct stratigraphic levels open upward into triangular zones of folding. Folding intensity and finite strain attenuates with distance from the fault tip. Trishear reproduces the bulk geometry and finite strain of the relatively homogeneous limestone sequence of the Rip Van Winkle anticline and predicts an initial location of the fault tip consistent with the field observations. Folding of the heterogeneous sedimentary section of La Zeta anticline, however, cannot be simulated by the trishear model alone. An additional mode of deformation involving transport of material from the backlimb into the hinge area and extension parallel to the direction of fault propagation is necessary to reproduce the geometry and finite strain of the anticline. Mechanical, distinct element modeling (DEM) of the anticlines indicates that their contrasting kinematics could have resulted from differences in mechanical stratigraphy and initial stress state. Folding of a homogenous, normally consolidated assemblage (initial horizontal to vertical stress ratio, $K_o = 1$) is trishear like and resembles the Rip Van Winkle anticline. Folding of a heterogenous (layered such as La Zeta), over-consolidated assemblage ($K_o > 1$) departs from the trishear model and resembles La Zeta anticline. Based on the DEM simulations, we postulate that the Rip Van Winkle anticline formed at high depths (high overburden loads and lithostatic stress conditions), and that La Zeta anticline formed at shallow depths, after substantial uplift and erosion of the Andean mountain front (which induced over-consolidation and high K_o).

Keywords: Fault propagation folding; Mechanical stratigraphy; Initial stress state; Trishear modeling; DEM modeling; Rip Van Winkle anticline; La Zeta anticline

1. Introduction

The processes of deformation in front of the tip of a propagating fault vary as function of the mechanical properties of the rocks involved in the deformation (mechanical stratigraphy; Erickson, 1996) and the active stress field (Jamison, 1992). Fracture toughness, or the ability of the rocks to absorb fault slip by folding, is not constant, but varies spatially and temporally with mechanical stratigraphy (Chapman and Williams, 1985; Dominic and McConell, 1994) and as the fault-fold system and the stress field evolve (King and Yielding, 1984; Anderson, 1995). Multiple modes of folding operate in front of the fault tip. These modes occur simultaneously in rock units with dissimilar mechanical properties (Fisher and Anastasio, 1994; Erslev and Mayborn, 1997), or progressively as deformation evolves (Storti et al., 1997).

In this paper, we analyze two structures that superbly record the deformation in front of the tip of a propagating fault: the Rip Van Winkle anticline in the Hudson Valley fold–thrust belt (eastern New York, USA) and La Zeta anticline in the eastern piedmont of the Andes at 36°S latitude (southern Mendoza, Argentina). Detailed surveys of the folds and field observations illustrate the geometry of folding and the character of the strain. Comparisons of the fold geometries and strain fields with the predictions of the trishear kinematic model (Erslev, 1991;

* Corresponding author. Tel.: +47 5558 3693.
E-mail address: nestor.cardozo@cipr.uib.no (N. Cardozo).

0191-8141/$ - see front matter © 2005 Elsevier Ltd. All rights reserved.
doi:10.1016/j.jsg.2005.06.003

Allmendinger, 1998), as well as mechanical distinct element (DEM) simulations, provide insight into the processes that controlled the kinematics of folding of the structures.

One of the test cases, the Rip Van Winkle anticline, proves to be well represented by the trishear model. But the second test, La Zeta anticline, illustrates a case for which the trishear model is a poor representation. Based on mechanical DEM modeling of the anticlines, we conclude that differences in mechanical stratigraphy and initial stress cause the differences in fold geometry and kinematics. This paper shows the benefits of integrating kinematic and mechanical models in the study of fault propagation folding.

2. Case studies

The scales of the folds chosen for this study range from decameters (Rip Van Winkle anticline) to kilometers (La Zeta anticline). The Rip Van Winkle anticline developed in a relatively homogeneous sequence of limestones and La Zeta anticline developed in a more heterogeneous sequence of volcaniclastics, calcareous sandstones, limestones and gypsum. In both structures, the associated fault, the cutoff geometries, and the fold are exceptionally well exposed. The anticlines offer a unique opportunity to explore the effects of mechanical stratigraphy and initial stress (overburden load and tectonic stresses; Jamison, 1992) on fault propagation folding.

2.1. Field methods

The folds were surveyed to reconstruct their three-dimensional geometries. x, y, z coordinates of selected beds and prominent faults were measured using a laser rangefinder with integrated compass and inclinometer at the Rip Van Winkle anticline, and a hand held GPS with integrated altimeter at La Zeta anticline. Local surveys with a laser rangefinder and coordinates from a rectified aerial photo and a high-resolution (90 m) digital elevation model, were also used in La Zeta anticline. In both surveys, the errors on locations range from 0.5 to 2% times the width of the folds' outcrops. Bedding orientations were used to determine fold axis orientations. Plunge-projections depicting the true cross-sectional geometry of the folds were generated by projecting the x, y, z coordinates parallel to the fold axes. We concentrated on mesostructures (cleavage, veins, fault planes and joints) to estimate the strain fields of the folds. In the Rip Van Winkle anticline, intracrystalline strain is small compared with the estimated mesoscopic strain. In the forelimb of the anticline, shortening from calcite twining is about 5% (Harris and Van Der Pluijm, 1998, their sample j94-12), whereas shortening from line balance of minor folds is about 30% (see Section 3.1). In La Zeta anticline, field inspection suggests that fossils are undeformed, indicating low penetrative strain.

2.2. The Rip Van Winkle anticline

The Rip Van Winkle anticline lies within the Hudson Valley fold–thrust belt, a west-vergent fold–thrust belt of Siluro-Devonian rocks east of the Catskill Mountains, southeastern New York (Fig. 1; Marshak, 1986). The outcrops analyzed in this study are located along the NW–SE-trending Route 23, 1/2 km west of the intersection with the New York State Thruway in Leeds, New York (Figs. 1 and 2; Marshak, 1986, his fig. 4; Marshak, 1990, his stop 2A). The rocks involved in the deformation belong to the Lower Devonian Helderberg Group. The exposed units involved in the fold are in ascending order: the Kalkberg Formation (argillaceous lime wackestone and packstone with thin layers of black chert), New Scotland Formation (argillaceous lime wackestone), and Becraft Formation (lime grainstone) (Fig. 2). The cumulative thickness of these units is 60 m (Marshak and Engelder, 1985). At some time during their history, these rocks reached temperatures in excess of 200 °C, corresponding to a maximum burial depth of about 6 km (Epstein et al., 1977; Friedman and Sanders, 1982; Lakatos and Miller, 1983). However, it is unknown whether maximum burial occurred during or after deformation. The age of deformation is controversial, with available evidence indicating either a Late Devonian or a Late Carboniferous age (Marshak, 1986).

In the northern outcrop, the strata are folded into an

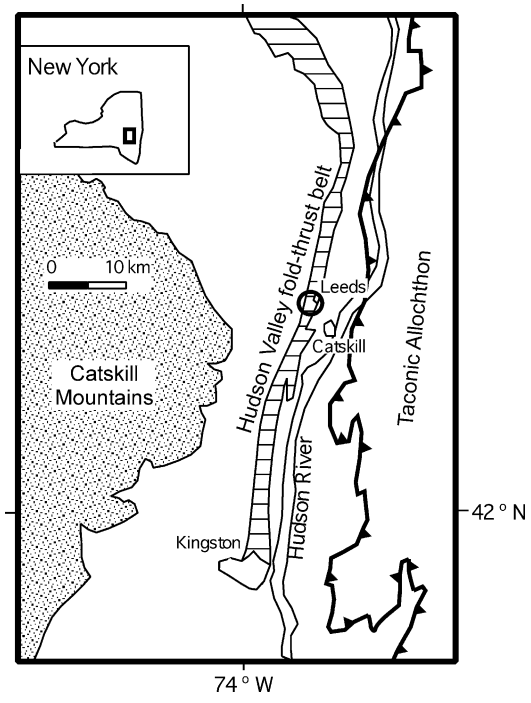

Fig. 1. Location map of the Rip Van Winkle anticline. Horizontal hatch pattern is the outcrop belt of Silurian through lower Middle Devonian strata of the Hudson Valley fold–thrust belt in eastern New York State. The barbed line is the western edge of the Taconic allochthon. Circled region includes the Rip Van Winkle anticline and structures along Route 23. Simplified from Marshak (1986).

a. Northern roadcut

b. Southern roadcut

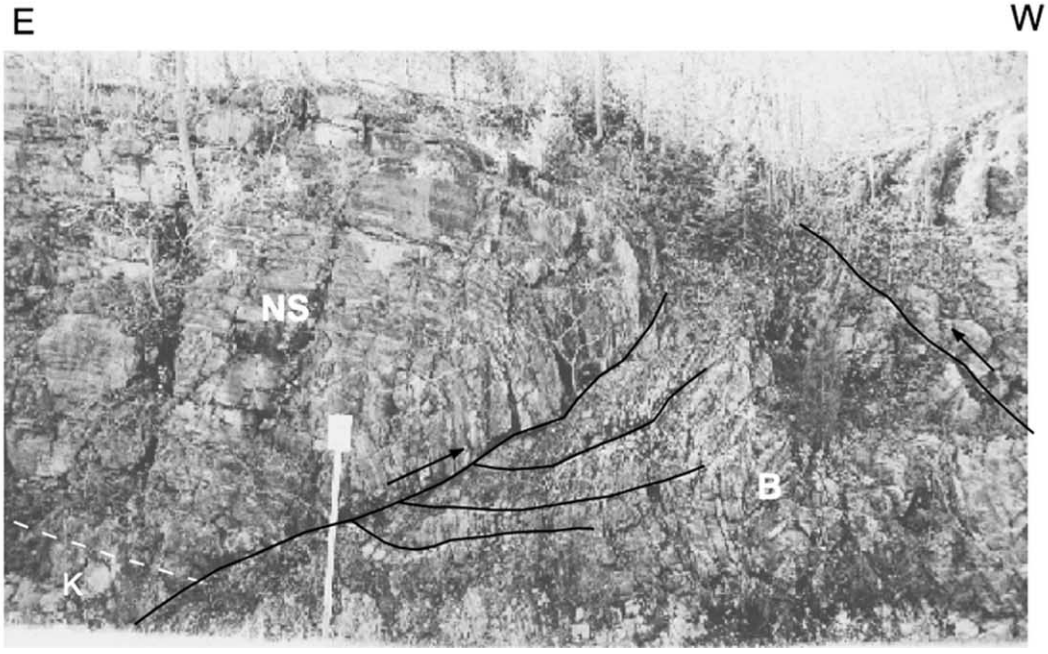

Fig. 2. (a) Northern and (b) southern outcrops of the Rip Van Winkle anticline along Route 23. Dashed white lines are formation contacts. Black lines are prominent faults with arrows indicating the sense of displacement. Outcropping formations, from oldest to youngest, are Kalkberg (K), New Scotland (NS), and Becraft (B). For scale, road pole on northern side is about 1.5 m and signal on southern side is about 3.0 m. In all figures, cross-sections are viewed to the south. The photo of the northern outcrop has been flipped to fit this standard.

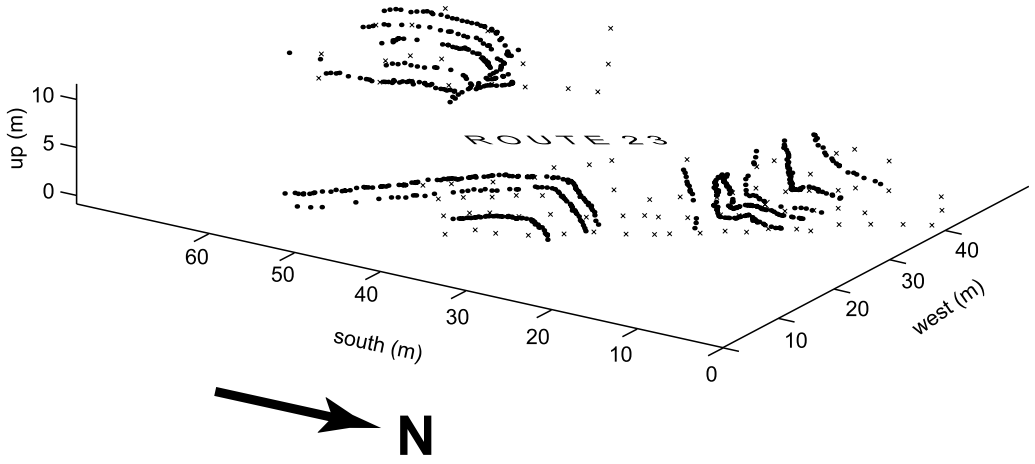

Fig. 3. 3-D geometry of the Rip Van Winkle anticline. Dots are surveyed points on selected beds and prominent faults. Crosses are surveyed points used as ground control points for rectification of the outcrop photographs (Fig. 2). Data were surveyed using a laser rangefinder. Maximum error on locations is 40 cm.

anticline–syncline pair (Figs. 2a and 3). In the southern outcrop, the anticline overlies a thrust fault (Figs. 2b and 3). Northern and southern outcrops are sections of a fold that formed and grew at the front of a propagating thrust (i.e. a fault propagation fold; Marshak, 1986). In the southern road cut, the forelimb steepens up-section (Figs. 2b and 3). Folding is not observed at or below the Kalkberg–New Scotland contact (Fig. 2b). This stratigraphic level is above the proposed décollement for the Hudson Valley fold–thrust belt (the Rondout detachment; Marshak, 1986). The fault could have propagated instantaneously from the Rondout detachment across the Kalkberg Formation (with no associated folding ahead of its tip), and slowed considerably on encountering the New Scotland Formation (causing folding of the rocks in and above this unit).

Poles to bedding indicate a fold axis trend/plunge of 036/1° (Fig. 4a). In the plunge projection, however, the bed of the northern (higher structural level) and southern (lower structural level) road cuts overlap. A steeper and more eastward fold axis (058/15°) is necessary to align the exposed hinge of the anticline in the northern and southern road cuts. This discrepancy may be due to a decrease in fault displacement from the southern to the northern road cut (see Section 3.1) or a conical fold geometry.

We chose to focus on the northern road cut, where the anticlinal geometry in front of the fault tip can best be observed (Figs. 2a and 3). Besides projecting the surveyed beds along the fold axis (white dots in Fig. 5), we transformed the photograph of the northern road cut (Fig. 2a) into a plunge-projection (grayscale image; Fig. 5). Surveyed locations on a grid (crosses in Fig. 3) were used as ground control points in the photo rectification. Close correspondence between the projected beds, bedding dips, and the rectified photo confirms the validity of this procedure (Fig. 5). The plunge-projection shows the nearly horizontal strata of the backlimb passing abruptly (in ~5 m) into the steeply dipping and locally overturned strata of the forelimb (Fig. 5). The tight syncline (minimum interlimb angle of 35°) opens up-section, and its core is cut by a west-vergent thrust (Fig. 5). The backlimb of the anticline is slightly rotated towards the east (Figs. 3 and 5).

Mesoscopic rock deformation (i.e. cleavage, minor fault planes and veins) is restricted to the forelimb of the anticline and the adjacent syncline. The lack of mesoscopic structures in the backlimb of the anticline suggests no material transport from forelimb to backlimb during folding. The distribution and morphology of mesoscopic structures depend on rock composition. Limestones with relatively high clay content (Upper Kalkberg and New Scotland Formations) preferentially developed cleavage, whereas limestones with little clay (Becralt Formation) preferentially developed calcite twinning (Marshak and Engelder, 1985).

Cleavage is stronger on steeply-dipping to overturned beds and adjacent to fault planes, where cleavage domains bend asymptotically into fault surfaces. Cleavage is inclined at low angles to bedding and becomes more parallel to bedding as bedding dip increases (right side of Fig. 4b). Veins are inclined at high angles to bedding and become more orthogonal to bedding as bedding dip increases (right side of Fig. 4c). Slickenlines on fault planes generally overprint cleavage-fault and veins-fault intersection lineations, but at some localities cleavage or veins cut the slickenlines. The above observations indicate that cleavage and veins developed early and throughout the evolution of the fold. This interpretation of cleavage formation early in the deformation sequence is further supported by the presence of cleavage in horizontal layers west of the Hudson Valley thrust belt (Engelder, 1979).

Fault planes parallel or cut bedding (Fig. 4d). Slickenlines are mostly perpendicular to the fold axis (Fig. 4d), suggesting minimum material transport along strike. Slickenline growth directions indicate shear towards the hinge of the anticline and out of the core of the syncline. Some faults are related to flexural slip during folding (Ramsay and Huber, 1987), whereas others appear to have

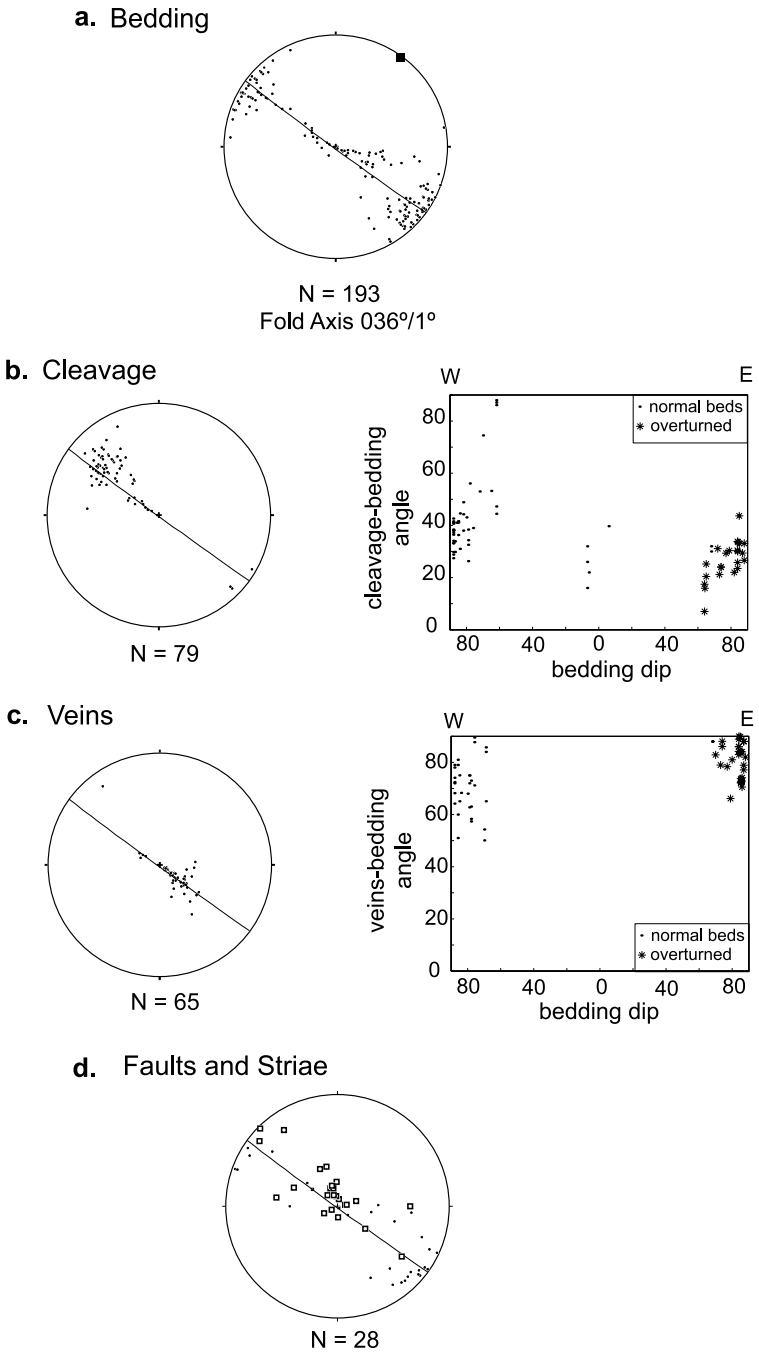

Fig. 4. Equal area, lower-hemisphere stereoplots of structural data collected in the Rip Van Winkle anticline along Route 23. (a) Poles to bedding. Square is the stereographically determined fold axis. (b) Poles to cleavage (left side) and cleavage-bedding angle across the structure (right side). (c) Poles to veins (left side) and veins-bedding angle across the structure (right side). (d) Poles to fault planes (dots), and slickenlines (squares). In (a)–(d), the great circle in stereoplot is the best cylindrical fit for the bedding data.

formed as a result of fold tightening (i.e. west-vergent thrust in the core of the syncline; Fig. 5).

Volumetric strain during folding is difficult to estimate. On the western limb of the Central anticline (~250 m west of the Rip Van Winkle anticline on Route 23) approximately 10% of the calcite was removed from the Kalkberg Formation, corresponding to a volume-loss strain of 5% (Marshak and Engelder, 1985). These data suggest nearly volume-constant deformation (Engelder and Marshak, 1985).

2.3. La Zeta anticline

La Zeta anticline is in the eastern foothills of the Andes at 36°S latitude, on the southern side of the Río Grande Valley, 4 km west of Bardas Blancas, southern Mendoza province,

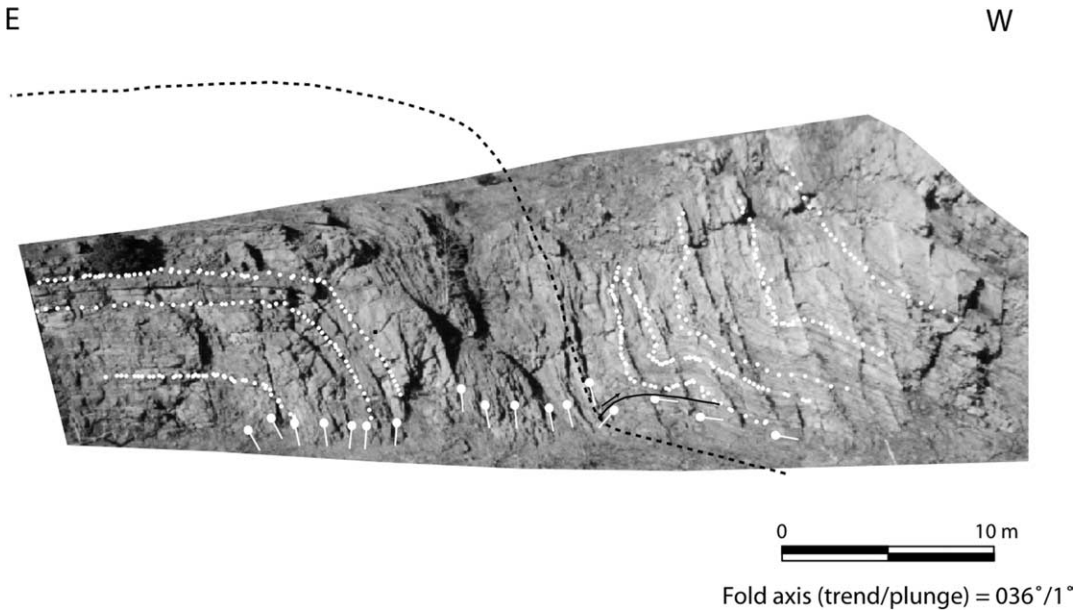

Fig. 5. Plunge-projection of the Rip Van Winkle anticline. White dots are surveyed beds on northern road cut, projected along the fold axis. Grayscale image is the rectified version of the photograph of the northern road cut in Fig. 2a for a coordinate system perpendicular to the fold axis. White dots with ticks are bedding dips at selected locations. Black line with arrow is the out of the syncline thrust. Black dashed line is the trial geometry used in trishear inverse modeling of the structure. Plunge projection has been flipped to maintain consistency in the orientation of view of the cross-sections.

Argentina (Fig. 6a and b). This 2-km-wide, west-vergent fold lies on the eastern flank of the Bardas Blancas anticline, a 20-km-wide, east-vergent structure formed by the emplacement of the Bardas Blancas blind thrust (Fig. 6b; Manceda and Figueroa, 1995; Dimieri, 1997). A tectonic wedge at the mountain front is formed by the east-vergent Bardas Blancas thrust and a west-vergent thrust nucleating from its leading edge (Fig. 6b; Dimieri, 1997; Manceda et al., 1990, 1992). West-vergent thrusts (backthrusts) decrease in dip towards the hinterland and detach from the Bardas Blancas thrust, deforming the wedge internally (Fig. 6b; Dimieri, 1997). La Zeta anticline grew in front of the backthrust closest to the leading edge of the Bardas Blancas thrust, the Río Grande backthrust (Fig. 6b and c).

La Zeta anticline is underlain by a basement sequence of Permo-Triassic volcanic breccias and porphyritic tuffs, and locally Lower Jurassic tuffaceous conglomerates (Choiyoi Group and Remoredo Formation, which we lump here as 'Choiyoi') (Figs. 6c and 7; Dessanti, 1973; Gulisano and Gutíerrez Pleimlig, 1994). The sedimentary cover consists of Middle–Upper Jurassic calcareous sandstones (Bardas Blancas Formation, ~150 m thick), limestones (La Manga Formation, ~70 m thick), and gypsum (Auquilco Formation, ~10 m thick) (Figs. 6c and 7; Gulisano and Gutíerrez Pleimlig, 1994). Miocene diorite porphyries intrude this sequence (Cerro Palao Mahuida; Fig. 7; Dessanti, 1973; Ramos and Nullo, 1993). Erosion contemporaneous with deformation removed about 2 km of strata (Mendoza to Malargüe Groups; Manceda and Figueroa, 1995; Manceda, personal communication).

The age of La Zeta anticline is closely related to the age of the Bardas Blancas thrust. Synorogenic strata onlapping the forelimb of the Bardas Blancas anticline suggests a middle to late Miocene age of deformation (Manceda, personal communication). Inside the tectonic wedge, gentler backthrusts towards the hinterland favor a hinterland-breaking sequence, in which the Río Grande backthrust and La Zeta anticline are the oldest structures (Dimieri, 1997).

On the southern side of the Río Grande Valley and along the trace of the Río Grande backthrust, the Choiyoi units overthrusts the Bardas Blancas Formation (Figs. 6c and 7). The fault can be traced up to the Choiyoi–Bardas Blancas hanging wall cutoff, where it opens upward into a diffuse zone of brittle deformation (Figs. 6c and 7). At the outcrop scale, it is not possible to locate precisely the fault tip. Fault displacement decreases as folding increases up-section. In front of the fault, a spectacular Z-like anticline–syncline pair formed in La Manga Formation (Figs. 6c and 7). The backlimb of the anticline and the western limb of the syncline are planar and dip an average of 20° to the SSE and 30° to the SE, respectively (Fig. 6c). The backlimb, however, rotates towards the east close to the hinge of the anticline, where several normal faults disrupt its continuity (Fig. 6c). The forelimb of the anticline is curved and steepens as it approaches the fault tip. Close to the fault tip, it is overturned and dips an average of 30° SE (Fig. 6c). The anticlinal hinge geometry changes from angular to rounded up-section. In the lower beds of La Manga Formation, at a zone of extreme deformation where the axial surface trace is laterally offset (Fig. 6c), the transition from the backlimb to the overturned forelimb occurs in less than 10 m. Farther

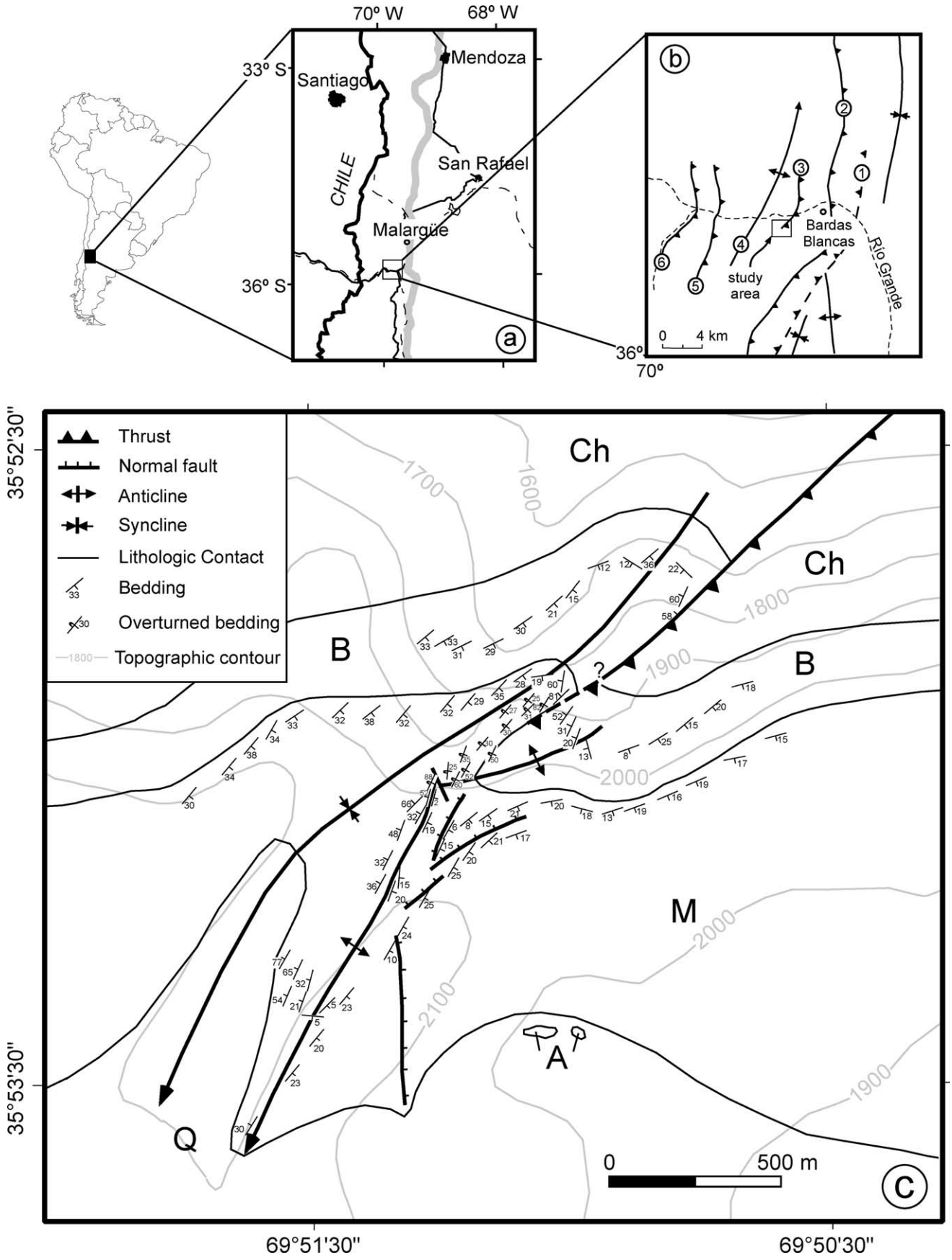
70º W
68º W
33º S
36º S
Santiago
Mendoza
San Rafael
Malargüe
CHILE
a
b
Bardas Blancas
study area
Río Grande
0 4 km
36º
70º
Thrust
Normal fault
Anticline
Syncline
Lithologic Contact
Bedding
Overturned bedding
Topographic contour
Ch
B
M
A
Q
1700
1600
1800
1900
2000
2100
0 500 m
c
35°52'30"
35°53'30"
69°51'30"
69°50'30"

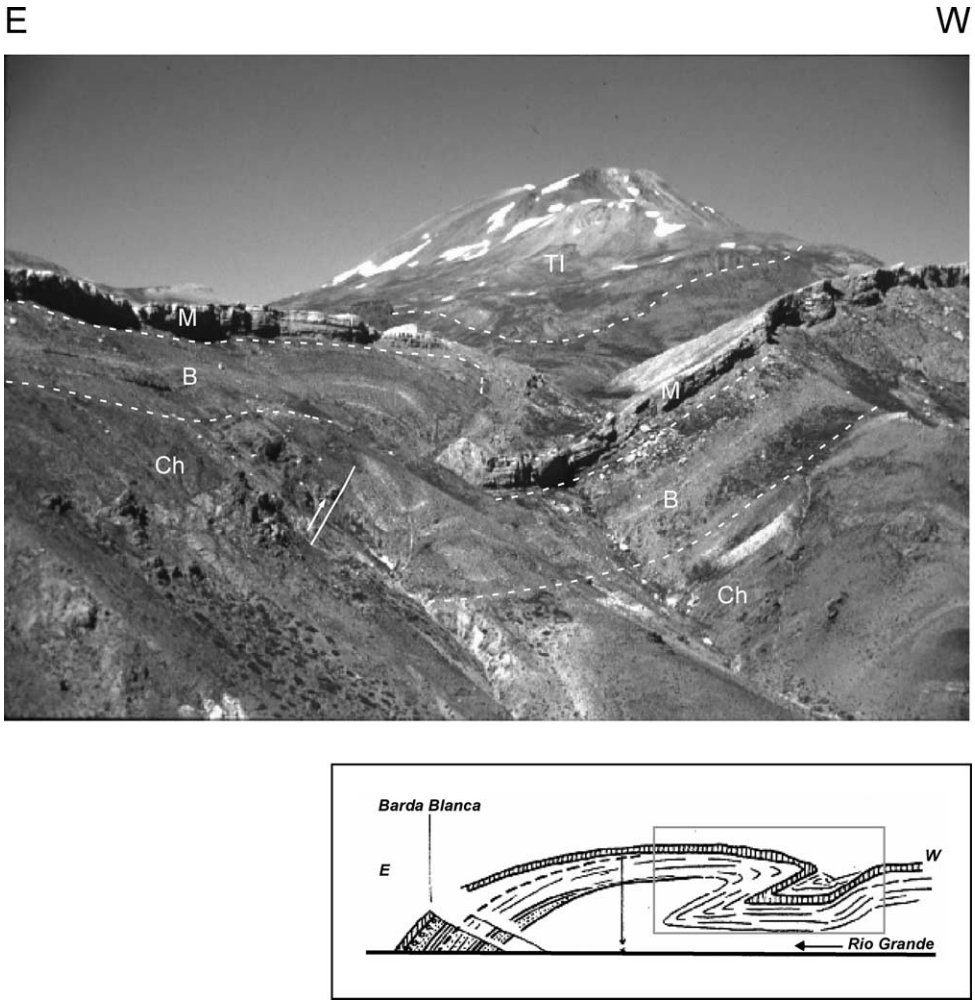

Fig. 7. Photograph of La Zeta anticline on the southern side of the Río Grande Valley. Dashed white lines are formation contacts. White line is the Río Grande backthrust with the arrow indicating the sense of displacement. Labels as in Fig. 6. TI, Tertiary Intrusives of the Cerro Palao Mahuida. The width of the view is approximately 2 km. Inset shows the first published schematic profile of the structure by Groeber (1918).

south and up-section at the top of La Manga Formation, that transition takes place over ~200 m (Fig. 6c).

To characterize fully the three-dimensional geometry of La Zeta anticline, x, y, z coordinates of the basement-cover contact, beds in the Bardas Blancas and La Manga Formations, the Río Grande backthrust, and prominent faults, were obtained (Fig. 8). Poles to bedding indicate a fold axis trend/plunge of 208/5° (Fig. 9a). The agreement between bedding traces and bedding dips in the plunge projection confirms that the fold has an approximately cylindrical geometry (Fig. 10). However, due to normal faulting of the backlimb (Fig. 6c), anticlinal hinge locations in upper beds of La Manga Formation (not shown in Fig. 10) and lower beds do not align.

In the plunge projection, the backlimb dips gently to the east (Fig. 10). Bedding traces and bedding dips differ mostly in this area. The western limb of the syncline rises as a result of displacement on La Guanaca backthrust farther west (Figs. 6b and 10; Manceda, personal communication). The Río Grande backthrust shallows up-section (Fig. 10). The basement-cover contact is barely folded, suggesting that the fault started to propagate close to this stratigraphic level (Fig. 10). Intense fold tightening and thickening of the hinge of the anticline occurs in the upper part of the Bardas Blancas Formation. Thickening of the hinge of the syncline is achieved by minor scale folding (Fig. 10). In the lower beds of La Manga Formation, the hinge geometry is angular in the anticline and rounded in the syncline, and the forelimb

Fig. 6. (a) Location of La Zeta anticline. Thick gray line indicates the eastern piedmont of the Andes. (b) Simplified structural map of the area. (1) Bardas Blancas thrust, approximate trace of leading branch line, (2) roof thrust of tectonic wedge, (3) Río Grande backthrust, (4) Bardas Blancas anticline, (5) La Guanaca backthrust, (6) Potimalal backthrust. From Dessanti (1973), Manceda et al. (1990) and Dimieri (1997). (c) Geologic map of the study area. Outcropping units from oldest to youngest are Choiyoi (Ch, which includes the Choiyoi Group and the Remoredo Formation), Bardas Blancas (B), La Manga (M), and Auquilco (A) Formations. Q, Quaternary. Topographic contours in meters above sea level.

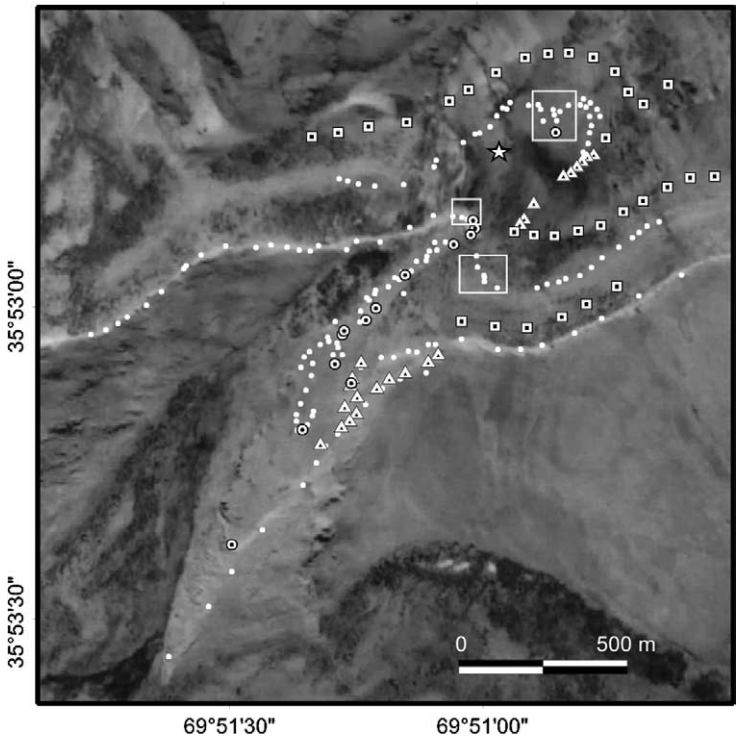

Fig. 8. La Zeta anticline survey. Dots are locations on selected beds and triangles are locations on faults, surveyed with a hand-held GPS and an altimeter. Star is the base station used for altimeter calibration. Squares are locations with coordinates from a geo-referenced aerial photo (gray image) and altitude from a high-resolution elevation model. Areas delimited by the white squares were also surveyed with a laser rangefinder. Circles with dots are locations with detailed measurements of joints and veins.

of the anticline is curvilinear and mostly overturned (Fig. 10). Thinning of the forelimb cannot be conclusively determined with the available data. Relatively poor exposure of the hinge and forelimb of the anticline prevents tracing beds continuously along the fold. A reasonable reconstruction of the fold indicates about 20% thinning of the forelimb (Fig. 10).

Rock deformation is notorious in the forelimb of the anticline, and the anticlinal and synclinal hinge areas (compare the prominent cliffs in the backlimb of the anticline and western limb of the syncline with the shattered forelimb in Fig. 7). The deformation is more intense in the hinge areas, suggesting fold growth by progressive rotation of its forelimb with some hinge pinning. The distribution of deformation reveals a marked variability of behavior of the strata during fault propagation, with deformation occurring preferentially in the upper part of the Bardas Blancas Formation and the lower part of La Manga Formation.

Mesoscopic structures include joints, veins, and fault planes (Fig. 9b–d). Stylolites and penetrative cleavage were not observed. Joints are mostly perpendicular to bedding (Fig. 9b). E–W and N–S joint sets (alter bed dip removal), parallel and perpendicular to the Río Grande Valley, occur in structural levels far from the fault (m1, m2–3, m4, Fig. 11). Some of these joints maintain a constant orientation across the structure, clearly postdating folding (Fig. 9b). We interpret these two sets to have been created by release of the overburden load, during or after the late stages of folding. Cross-fold (ENE–WSW) and fold-oblique (NNW–SSE) joint sets become apparent down-section as the anticline tightens and the fault is approached (m2–3, m5, Fig. 11). These sets also occur in the footwall syncline in the Bardas Blancas Formation (m9, Fig. 11). We interpret these sets either to predate or be synchronous with folding. Veins are perpendicular, oblique, or parallel to bedding (Fig. 9c). Veins are abundant close to the fault, in the forelimb of the anticline and in the hinge of the syncline (m6–7, m8, Fig. 11). Two vein sets strike parallel and perpendicular to the fold axis (m8, Fig. 11). Veins perpendicular to bedding, offset along bedding-parallel fault planes, indicate shear out of the core of the syncline.

Fault planes and striae are randomly oriented with respect to the fold axis (Fig. 9d). Along the trace of the Río Grande backthrust, striae were not observed. Folding is continuous at the map scale of La Zeta anticline, but at a mesoscopic scale, it is probably accomplished by the collective movement of blocks on a population of fractures (cataclastic flow of Ismat and Mitra (2001)).

3. Kinematic modeling

Common attributes characterize the Rip Van Winkle and La Zeta anticlines. In both structures: (1) faults nucleating

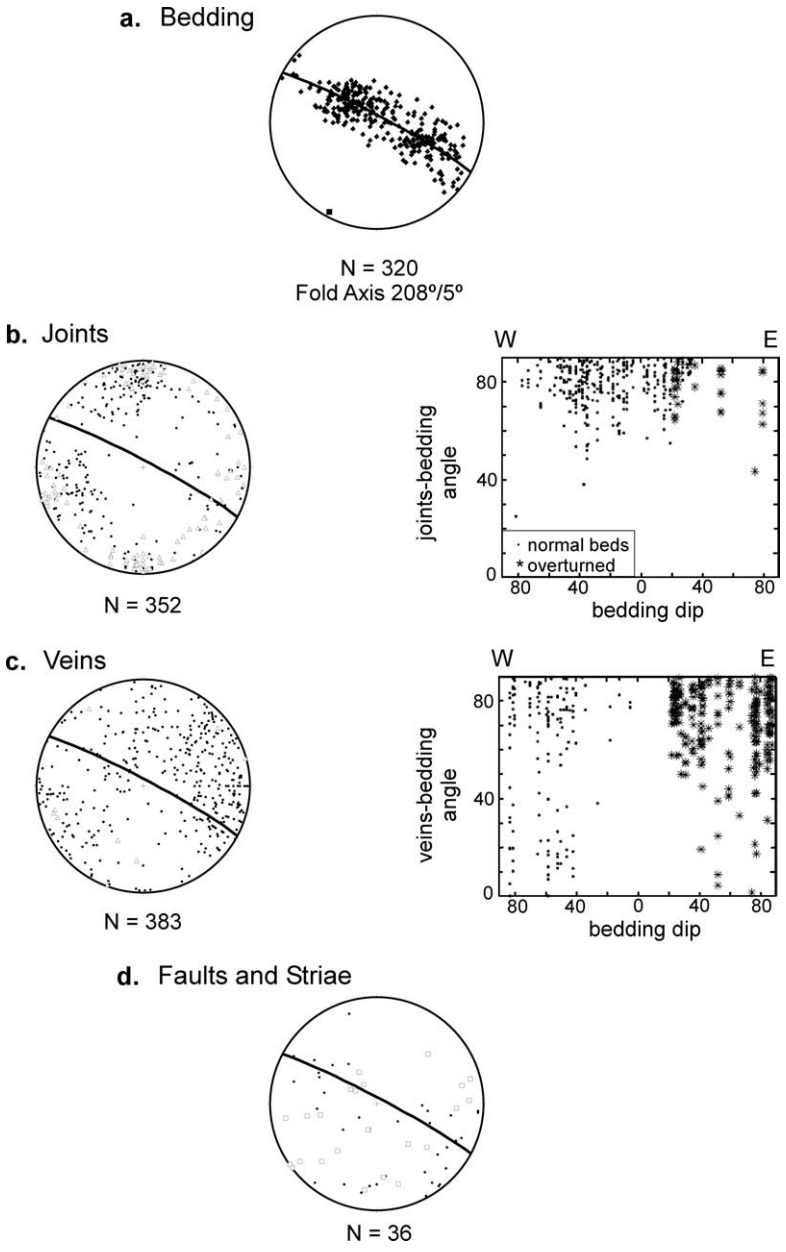

Fig. 9. Equal area, lower-hemisphere stereoplots of structural data collected in La Zeta anticline. (a) Poles to bedding. Square is the stereographically determined fold axis. (b) Poles to joints (left side) in the fold's backlimb (triangles) and fold's forelimb (dots), and joints-bedding angle across the structure (right side). (c) Poles to veins (left side) and veins-bedding angle across the structure (right side). (d) Poles to fault planes (dots), and slickenlines (squares). In (a)–(d), the great circle in stereoplot is the best cylindrical fit for the bedding data.

from distinctive interfaces open upward into diffuse zones of folding, (2) planar, undeformed backlimbs abruptly pass to curved forelimbs that steepen towards the fault, and (3) hinge areas open up-section. Fold geometry and finite strain change with structural level and proximity to the fault. Trishear, or distributed shear in a triangular zone focused at the tip of a propagating fault (Erslev, 1991; Allmendinger, 1998), has been proposed to simulate such structural features. In this section, we test the success of the trishear kinematic model in reproducing the geometry and finite strain of the anticlines.

3.1. The Rip Van Winkle anticline

The plunge projection of the northern road cut (Fig. 5) was used to model the anticline. Although the geometry of the anticline varies in three dimensions (i.e. fault slip decreases from south to north), the use of the plunge projection is justified by the fact that minimum material transport occurs along the fold axis (Section 2.2). We do not know the mechanism by which fault slip varies along strike, but we know that most of the deformation is concentrated in the plunge projection.

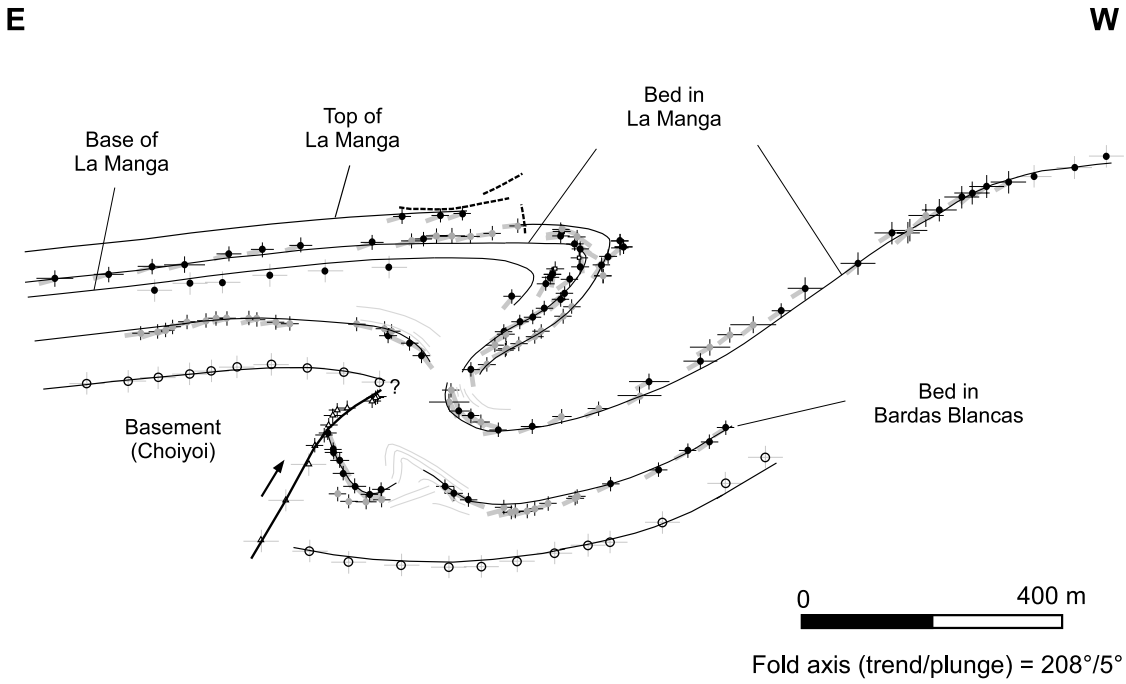

Fig. 10. Plunge-projection of La Zeta anticline. Triangles are locations on the Río Grande backthrust, circles are locations on the basement-cover (Choiyoi–Bardas Blancas) contact, black and gray dots are locations on selected beds, and squares are locations on the hinge of the anticline. Crosses are error bars, gray in locations with coordinates from a referenced aerial photo and a high-resolution elevation model. Gray ticks are bedding dips. Gray lines are bedding traces in areas surveyed with a laser rangefinder.

Trishear modeling involves two steps: (1) a grid search of the parameters that best restore the fold to its initial, planar geometry, (2) forward modeling of the geometry and strain of the structure using the parameters of the best-fit model (Allmendinger, 1998). To find the best-fit model, the inverse trishear algorithm computes the proximity of the restored geometry of one bed in the section to a straight line (Allmendinger, 1998). In the outcrops of the Rip Van Winkle anticline, however, no single bed is exposed across the entire structure. Hence, we used a trial, reasonable geometry for a bed close to the New Scotland–Becraft contact (black dashed line, Fig. 5). Fault dip is known in the structure. The fault dips 25°E in the southern road cut (Fig. 2b). The grid search parameters are: fault propagation to fault slip ratio (*P*/*S*, from 1.0 to 2.0 in steps of 0.1), apical angle of the triangular zone (trishear angle, from 60 to 120° in steps of 2°), fault slip (from 0 to 80 m in steps of 1 m), and the current position of the fault tip in a 10 by 10 m region close to the core of the syncline. The model that best restores the fold has a *P*/*S* of 1.5, a trishear angle of 90°, and a slip of 43 m.

Forward modeling using the best-fit parameters produces a geometry remarkably similar to that of the fold (Fig. 12). The fit is less accurate in the western side of the section, probably due to the interference of east-vergent folds and thrusts immediately west of the Rip Van Winkle anticline (Figs. 2a and 12; Marshak, 1986, his fig. 4a). Trishear replicates the overall thickening of the hinge of the syncline. However, the model cannot reproduce the folding and faulting of the Becraft Formation in the core of the syncline (Fig. 12). Trishear provides a bulk description of the deformation, but dictates nothing about the specific structures by which this deformation was accomplished (Allmendinger, 1998).

Trishear predicts an initial location of the fault tip close to the Kalkberg–New Scotland contact (inset Fig. 12). In agreement with the observations of the southern road cut, folding in the model occurs above this stratigraphic level (Fig. 2b). The predicted final location of the fault tip is close to the New Scotland–Becraft contact and the maximum stratigraphic throw is less than the thickness of the New Scotland Formation (inset Fig. 12). In the southern road cut, however, the fault propagates through the Becraft Formation and the maximum stratigraphic throw is greater than the thickness of the New Scotland Formation (Fig. 2b). Both fault slip and fault propagation decrease to the north, suggesting that the fault may have propagated up-section with a characteristic *P*/*S* ratio, and northward along strike.

The strain field of the forward trishear model is close in orientation and in magnitude to the strain field of the anticline (Fig. 13). In domains 1 and 2 (gray rectangles in Fig. 13) the predicted maximum and minimum principal strain axes are subparallel to cleavage and veins, respectively (Fig. 13a). Trishear maximum principal strain axes do not coincide with cleavage in domain 3 (Fig. 13a). Cleavage in domain 3 is associated to out of the syncline thrusting. However, there is an exceptionally good fit between the trishear predicted stretch along the minimum principal strain axis (Str), and the stretch estimated from line balance of tight folds in the Becraft Formation (Sf; Fig. 13a).

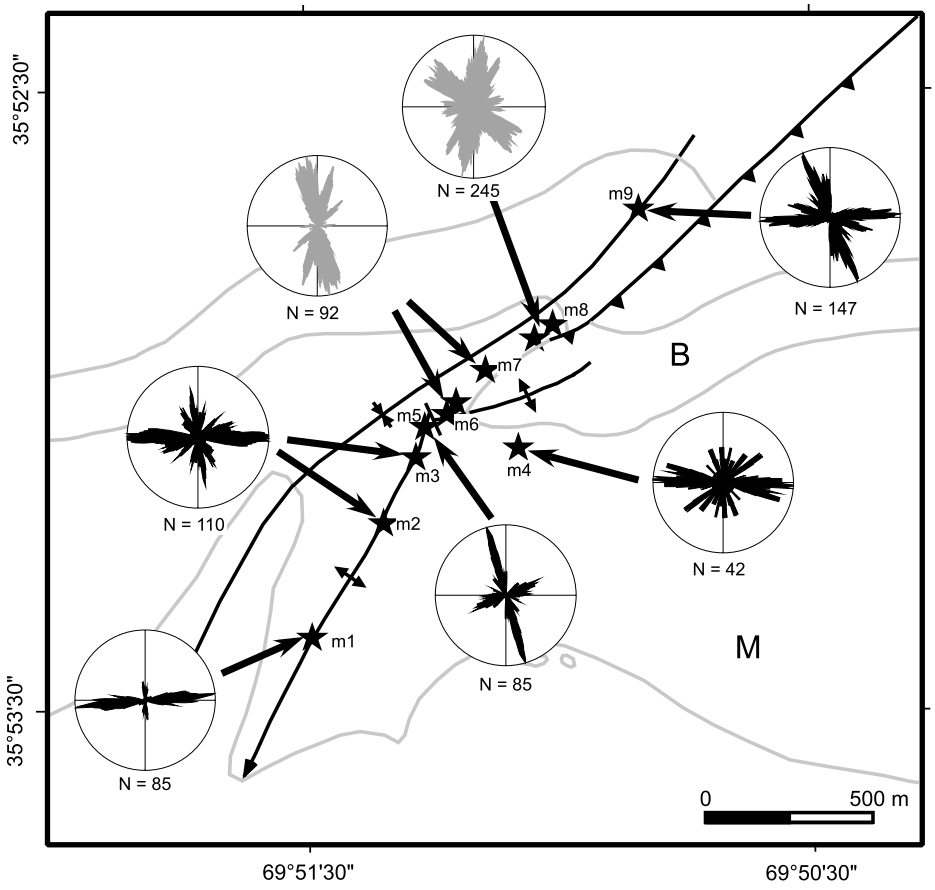

Fig. 11. Rose diagrams of the strike of joints (black) and veins (gray) in La Zeta anticline, after bed dip removal. m, station, *N*, number of measurements. Each rose diagram is symmetric and has been smoothed using a 10° interval.

Trishear does not replicate the minor structural orientations of domain 3, but succeeds in predicting the bulk strain.

The lines of no finite elongation (LNFE) from the trishear model are proxies for shear planes (Allmendinger, 1998). LNFE are consistent with the orientation of minor fault planes in the forelimb of the anticline (Fig. 13b). The set of LNFE antithetic to the main fault parallel the minor fault planes in domains 1 and 2 (Fig. 13b). Similar to the real structure, the predicted fault planes are locally parallel to bedding (Fig. 13b). The best-fit trishear model suggests that the faults formed during a late stage of folding, when the set of LNFE antithetic to the main fault paralleled bedding. The overprinting of cleavage-fault and veins-fault intersections by slickenlines on fault surfaces favors this assumption. However, this hypothesis cannot be tested without data on incremental strain histories. The LNFE are inconsistent with the orientation of fault planes in domain 3. In this domain, the sense of displacement of the fault planes is mostly out of the core of the syncline (Fig. 13b).

3.2. La Zeta anticline

No unique combination of trishear parameters can adequately reproduce the geometry of La Zeta anticline. Fold tightening and thickening of the hinge of the anticline, and the rounded geometry of the hinge of the syncline in the Bardas Blancas Formation–lower part of La Manga Formation (Fig. 10), cannot be simulated with a single trishear model. Tightening of the anticline can be reproduced by a trishear model with a fault that propagates through the Bardas Blancas Formation with decreasing trishear angles. Thickening of the hinge of the anticline can be enhanced by concentrating the deformation towards the center of the triangular zone (i.e. high concentration factor of Zehnder and Allmendinger (2000), which is equivalent to the heterogeneous trishear model of Erslev (1991)). However, decreasing trishear angles and/or high concentration factors fail to replicate the observed amount of hinge thickening. The main deficiency of trishear is the inability to model the heterogeneous, layered character of the sedimentary section. As the fault propagates through the Bardas Blancas Formation, transport of material from the backlimb into the hinge area (i.e. backlimb, layer parallel slip; Erslev and Mayborn, 1997), and extension parallel to the direction of fault propagation are necessary to get the thickening of the anticlinal hinge. Transport of material from the backlimb into the hinge area is impossible to accomplish with trishear, since the model assumes rigid hanging wall

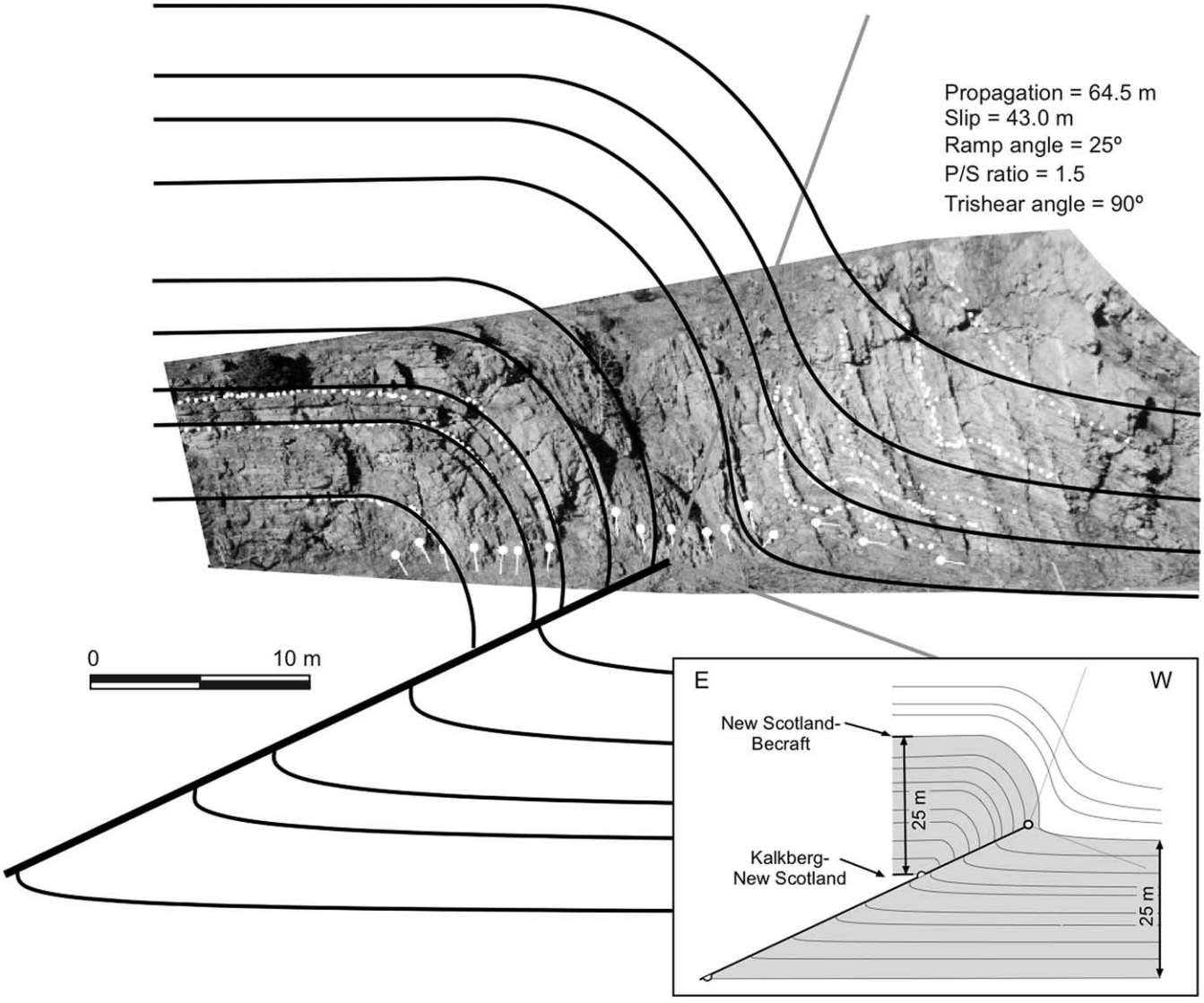

Fig. 12. Trishear modeling of the Rip Van Winkle anticline. The best-fit trishear model (black thick lines) is superimposed on the fold's plunge-section (grayscale image). White dots are surveyed beds, projected into the section. White dots with ticks are bedding dips. Inset shows the agreement between the predicted initial location of the fault tip and that suggested by field observations. Half circles indicate the initial location of the fault tip (in the hanging wall and footwall). White circle indicates the final location of the fault tip. The thickness of the New Scotland Formation (gray polygon) is from uniform dip sections east of the Rip Van Winkle anticline (Marshak, 1990, his plate 2).

translation parallel to the fault (Zehnder and Allmendinger, 2000).

4. Mechanical modeling

Physical processes determined the kinematics of the Rip Van Winkle and La Zeta anticlines. In this section, we use a two-dimensional DEM to explore the mechanics of folding of the anticlines. In the model, the solid is represented by an assemblage of rigid, frictional, linear-elastic, circular particles that displace independently from one another and interact at contacts between the particles according to fundamental laws of physics. At particle contacts, the constitutive behavior is represented by springs in compression and shear, and a slip model that allows particle slip whenever the ratio between the shear and normal contact forces is greater than the particle friction. Particle rolling is not allowed in the model. Details about the laws of particle interaction and the strategy for calculating the deformation and bulk mechanical properties of the assemblage are given in Morgan and Boettcher (1999) and Morgan and McGovern (2005). Strayer and Suppe (2002) and Finch et al. (2003) have also studied contractional fault propagation folding using the DEM.

Fig. 14 shows the configuration of the mechanical model. A 6000 by 1000 m consolidated assemblage is subjected to faulting along a 30° reverse fault. The model consisted of two stages of deformation: consolidation and faulting. During the consolidation stage the assemblage was created

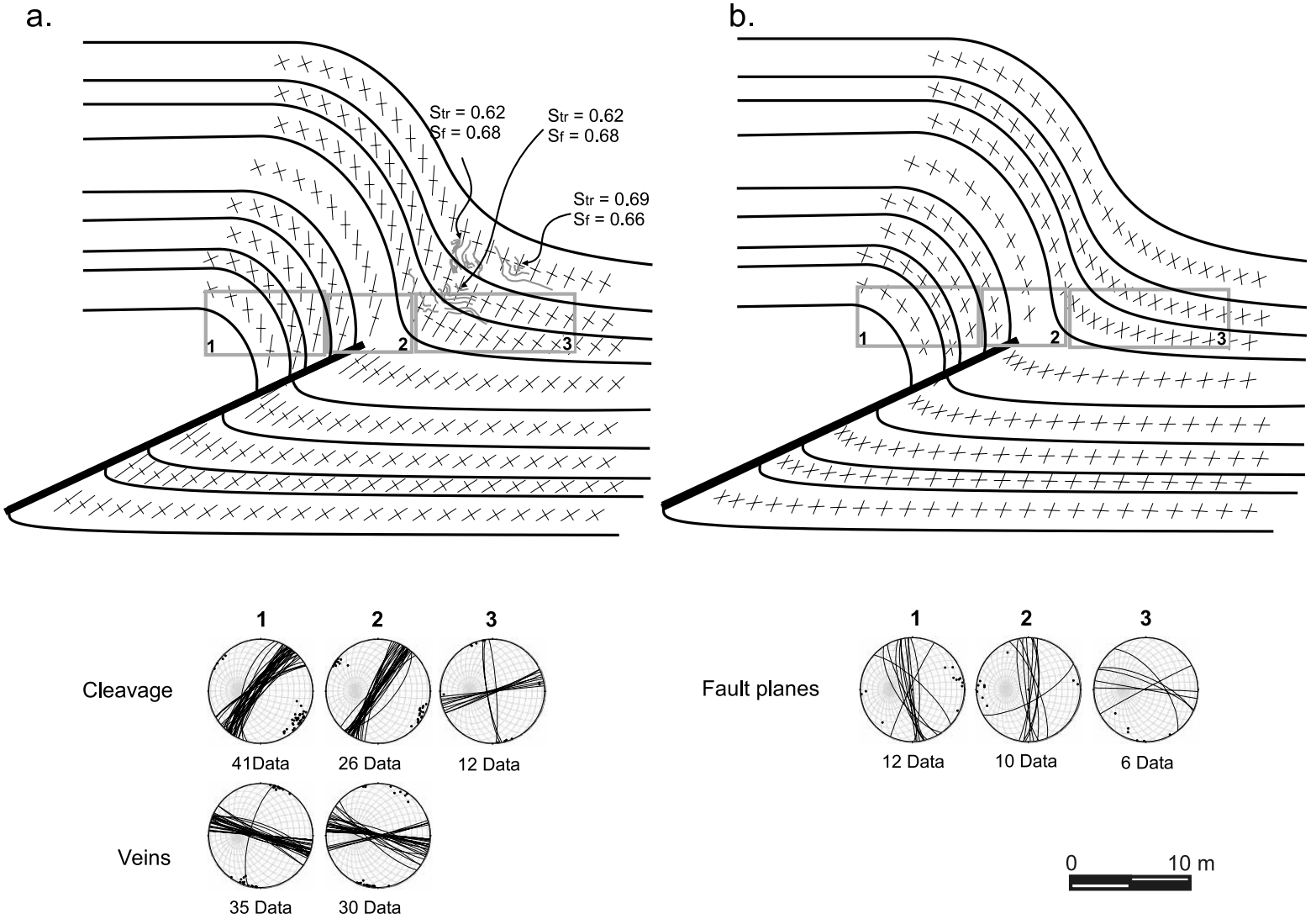

Fig. 13. (a) Comparison of trishear predicted principal strain axes (ticks in cross pattern) and cleavage and veins (equal area stereoplots) in the Rip Van Winkle anticline. Long and short ticks are trishear maximum and minimum principal strain axes, respectively. Also shown is the match between trishear predicted stretch along the minimum principal strain axis (Str) and the stretch estimated from line balance of tight folds (gray lines) in the Becraft Formation (Sf). (b) Comparison of trishear predicted lines of no finite elongation (ticks in cross pattern) and fault planes (equal area stereoplots). Stereoplots are viewed in the same orientation as the cross-sections. The great circles of the underlying net (light gray) converge towards the north (0, 0) direction.

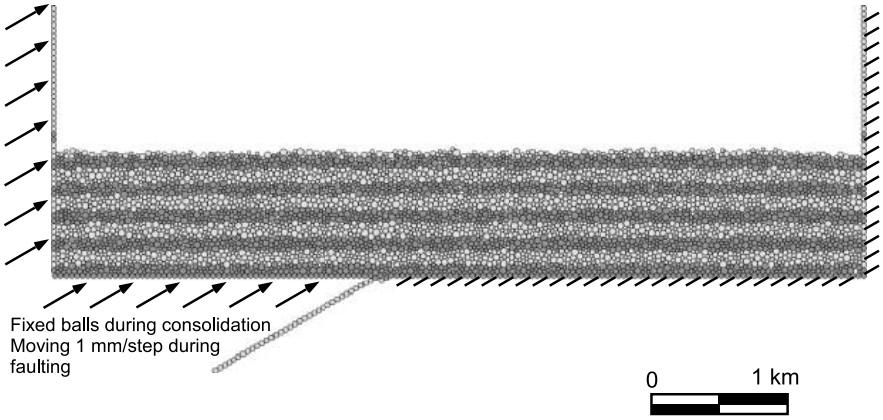

Physical parameters for simulations

Parameter	Value
number of particles	5080
particle sizes	15, 20 and 25 m
particle density	1000 kg/m^3
shear modulus	29 GPa
Poisson's ratio	0.20
interparticle friction (isotropic)	0.28
gravity	10 m/s^2

Fig. 14. Configuration of the mechanical simulations. Inset shows the physical and numerical parameters for the simulations.

by randomly generating 5000 particles of three sizes: 25, 20, and 15 m, within a two-dimensional, rectangular domain delimited by fixed balls (Fig. 14). The range of particle sizes was chosen to prevent formation of ordered packings, which could restrict the fault geometries. Particle densities are set at 1000 kg/m^3, a value that accounts for the buoyant density of saturated rocks, with a dry bulk density of about 2000 kg/m^3, representative of shallow sediments. Shear modulus is 29 GPa, and Poisson ratio is 0.2 (inset Fig. 14). The assemblage was consolidated following two strategies. In the first strategy, the assemblage was consolidated under normal gravity (10 m/s^2). At the end of consolidation, the maximum principal stress was oriented vertically and the ratio between the horizontal and vertical stresses (K_o) was less than 1, consistent with a normal consolidation stress path (Lambe and Withman, 1979). In the second strategy, the assemblage was fully consolidated under high gravity (30 m/s^2), and then relaxed under normal gravity (10 m/s^2). This loading path is equivalent to burial of the sediment package beneath a thick overburden, followed by erosion. This induces a state of over-consolidation defined by an over-consolidation ratio (OCR) of 3. The enhanced particle packing of this assemblage leads to strong frictional bonds, which lock in high horizontal stresses. The K_o value is therefore greater than 1. During the faulting stage of deformation, the left side and base of the model were moved along a 30° direction, parallel to the fault plane, at a rate of about 1 mm per step (Fig. 14).

Fig. 15 shows the geometry resulting from fault propagation folding in a homogeneous, normally consolidated (Fig. 15a) or over-consolidated (Fig. 15b) sequence, after 900,000 steps (final fault slip = 900 m). The interparticle friction (μ_p) is set to 0.28 for all particles, which equates a bulk friction value (μ_b) of 0.5 (Morgan, 1999, 2004). Fault propagation folding in a homogeneous, normally consolidated sequence resembles the geometry of the Rip Van Winkle anticline. The resulting fold is trishear like (Fig. 15a). The fold geometry is very similar to that generated by Finch et al. (2003) in their DEM simulations (e.g. their fig. 5). Fault propagation folding in a homogeneous, over-consolidated sequence, however, resembles more the geometry of La Zeta anticline. The resulting fold departs from the trishear like geometry (Fig. 15b).

Plots of the cumulative gradient of the horizontal displacement field in the vertical direction (Fig. 16; Morgan and Boettcher, 1999), illustrate the evolution of the deformation. Areas darker or lighter than the background indicate discontinuities in the displacement field, which are representative of discrete slip surfaces or minor faults. In the homogeneous, normally consolidated assemblage (Fig. 16a) the deformation is more distributed than in the homogenous,

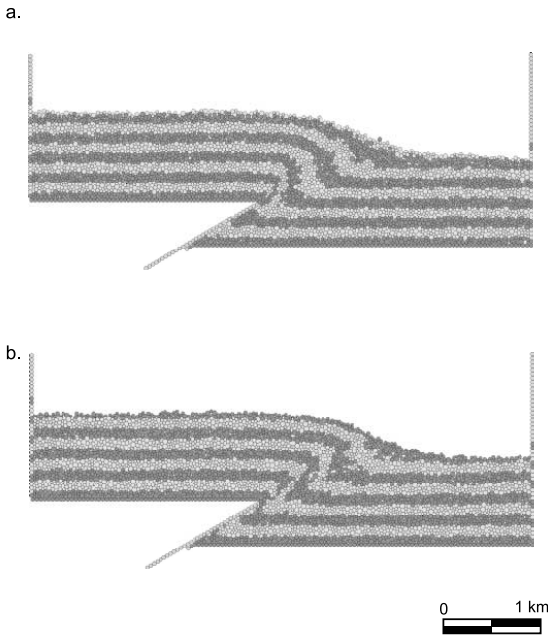

Fig. 15. Fault propagation folding of a homogeneous assemblage (interparticle friction $\mu_p = 0.28$). (a) Normally consolidated assemblage. (b) Over-consolidated assemblage (over-consolidation ratio = 3). Dark and light colors indicate initially horizontal markers. Final fault slip is about 900 m.

over-consolidated assemblage (Fig. 16b). In the normally consolidated assemblage the deformation is more or less equally distributed in the hanging wall and footwall areas (Fig. 16a). In the over-consolidated assemblage the deformation is localized along the fault (i.e. along the anticlinal hinge), and in a minor degree in the footwall (Fig. 16b). The strong frictional bonds created during the over-consolidation process induce localization of deformation (i.e. folding) along the fault. These simulations suggest that a low K_o (close to 1) existed at the onset of folding of the Rip Van Winkle anticline.

Fig. 17 shows the geometry resulting from fault propagation folding in a mechanically stratified (layers with different μ_p), normally consolidated (Fig. 17a) or over-consolidated (Fig. 17b) assemblage, after 900,000 steps (final fault slip = 900 m). To approximate the sedimentary sequence of La Zeta anticline, alternating layers were assigned μ_p values of 0.5 ($\mu_b = 0.8$) for the basement, 0.28 ($\mu_b = 0.5$) for the Bardas Blancas sandstones, 0.35 ($\mu_b = 0.6$) for La Manga limestone, 0.1 ($\mu_b = 0.2$) for the Auquilco gypsum, and 0.28 ($\mu_b = 0.5$) for the units above (Fig. 17). Fault propagation folding in the layered, normally consolidated sequence resembles the geometry of La Zeta anticline (Fig. 17a). Fault propagation folding in the layered, over-consolidated sequence also resembles La Zeta anticline, but additionally the model captures a characteristic feature of La Zeta anticline: similar to the actual structure, the anticlinal fold hinge geometry changes from angular at the base of the limestone to rounded at the transition limestone–gypsum (Fig. 17b and Section 2.3).

Fig. 18 illustrates the evolution of the deformation. The introduction of a heterogeneous, layered sequence such as the one of La Zeta anticline, results in localization of deformation along the anticlinal hinge area (compare Figs. 16a and 18a). Heterogeneity plus over-consolidation

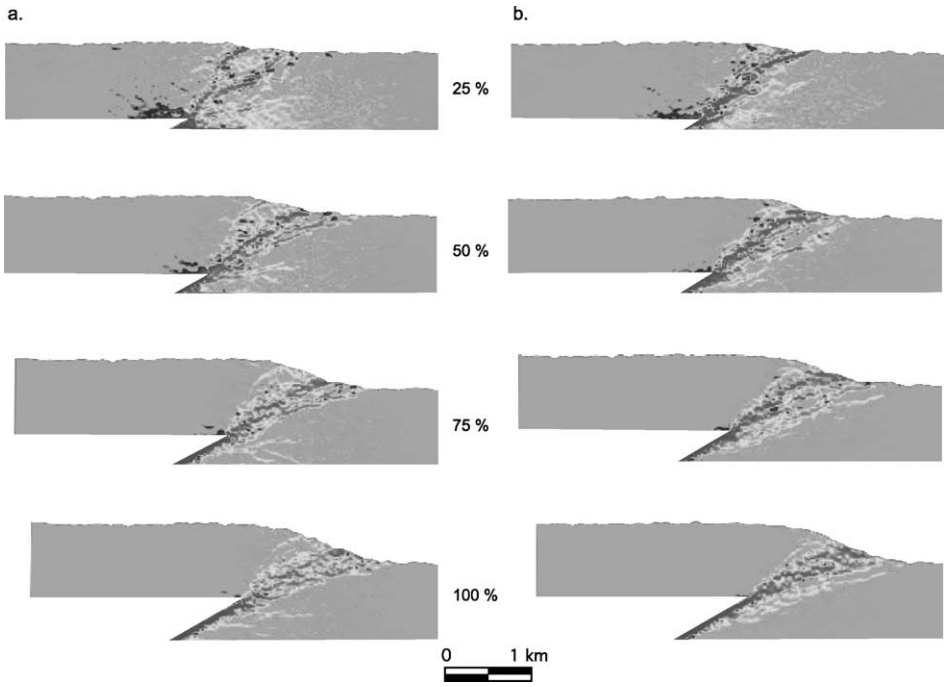

Fig. 16. Progression of deformation in the homogeneous assemblage. (a) Normally consolidated assemblage. (b) Over-consolidated assemblage. The nature of deformation is highlighted by the cumulative gradient of the horizontal displacement field in the vertical direction. Areas darker or lighter than the background indicate discontinuities in the displacement field (i.e. discrete slip surfaces or faults). The plots are shown at 25, 50, 75, and 100% of the final fault slip.

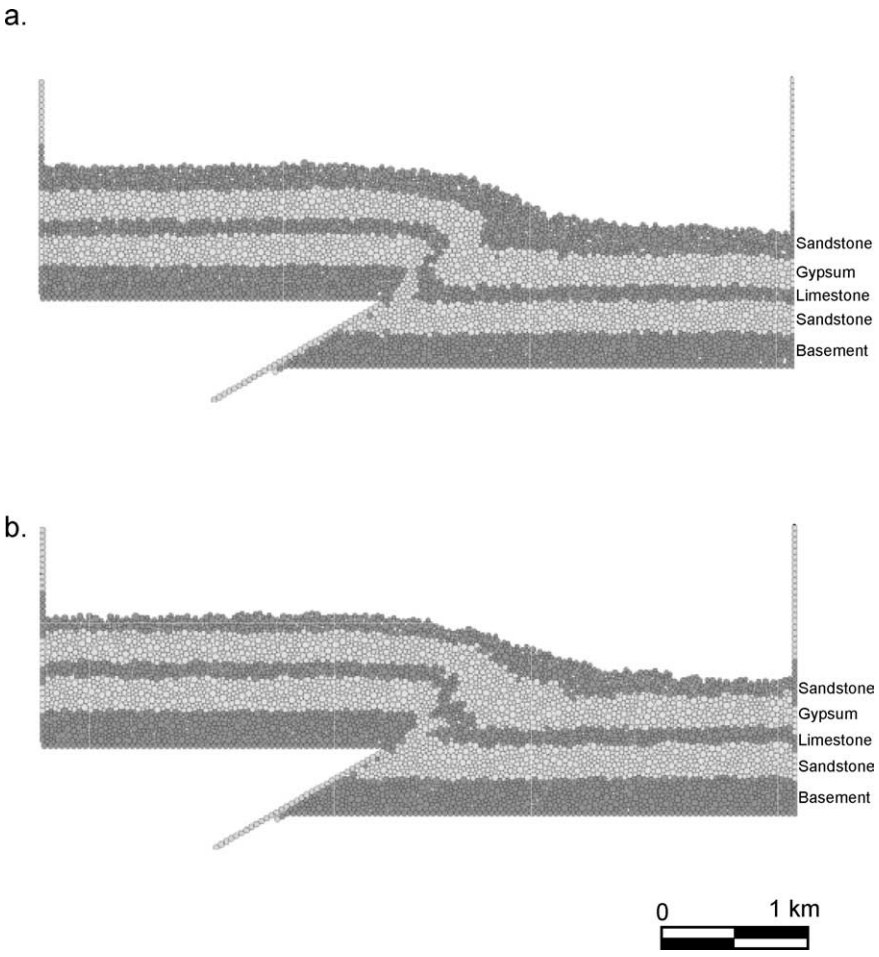

Fig. 17. Fault propagation folding of a heterogeneous, layered assemblage. (a) Normally consolidated assemblage. (b) Over-consolidated assemblage (over-consolidation ratio = 3). Dark and light colors indicate layers with different interparticle friction (μ_p). From bottom to top the layers are: basement ($\mu_p = 0.5$), sandstone ($\mu_p = 0.28$), limestone ($\mu_p = 0.35$), gypsum ($\mu_p = 0.1$), and additional cover ($\mu_p = 0.28$). Final fault slip is about 900 m.

results in localization of deformation along the anticlinal hinge in units below the limestone, and distributed deformation in units above the limestone (Fig. 18b). Over-consolidation therefore induces granular flow (i.e. folding) between layers that in the model behave brittlely (the basement and the limestone). These simulations suggest that two elements were critical in defining the distinct geometry of La Zeta anticline: the heterogeneity of the sedimentary sequence (mechanical stratigraphy), and an initial state of stress characterized by a high K_o, which enhanced folding of the Bardas Blancas Formation between the more competent Choiyoi Group and La Manga Formation.

5. Discussion

Multiple processes of deformation generated the structures studied here, with their influence dependent on mechanical stratigraphy and the stress state. In the relatively homogeneous section of the Rip Van Winkle anticline, bulk fold geometry and finite strain can be modeled by shear oblique to bedding (trishear). Locally, however, bedding parallel shear dominates as a consequence of the anisotropy imposed by bedding. These modes of deformation, which operate at different scales, are complementary rather than incompatible. The greatest success of trishear in the Rip Van Winkle anticline is the prediction of an initial location of the fault tip consistent with the observations. Northward decrease of both fault slip and fault propagation suggests that the fault propagated up-section with a characteristic P/S ratio. It also propagated northward along strike. A good fit in geometry and finite strain, however, does not uniquely constrain the kinematics of the structure (Fisher and Anastasio, 1994). Without incremental strain histories, it is impossible to test if the path of deformation of the trishear model that best fits the anticline is correct.

The predictable, trishear like deformation of the Rip Van Winkle anticline implies homogenous material subjected to ductile deformation (DEM simulations, Section 4). The Rip Van Winkle anticline is probably the result of fault propagation folding of a relatively homogenous sequence under initial low K_o conditions (K_o close to 1 or lithostatic stress conditions). Low K_o values (close to lithostatic stress conditions) are representative of relatively high depths

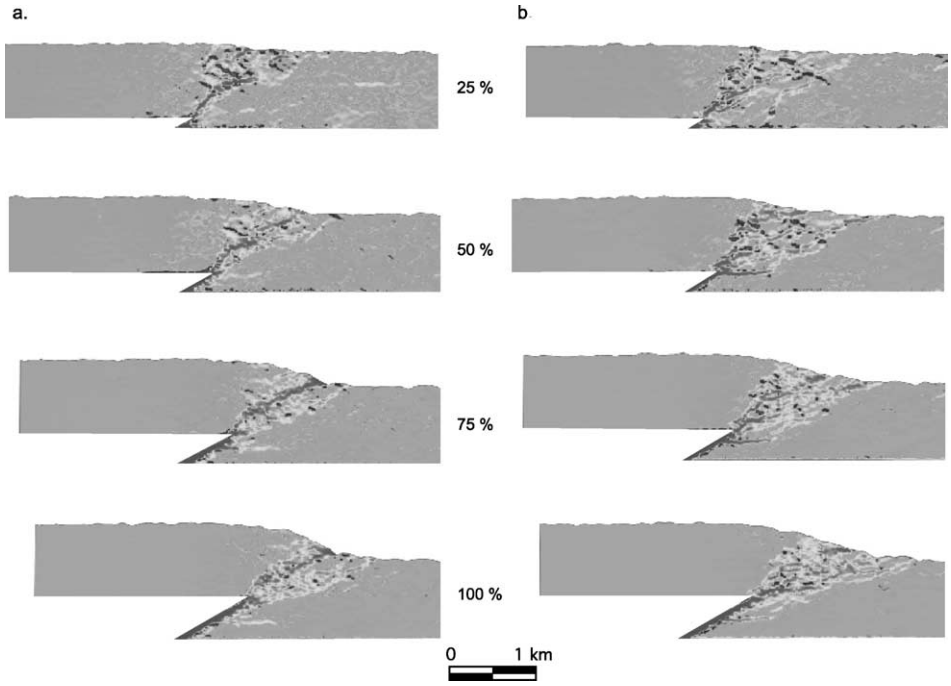

Fig. 18. Progression of deformation in the heterogeneous, layered assemblage. (a) Normally consolidated assemblage. (b) Over-consolidated assemblage. The nature of deformation is highlighted by the cumulative gradient of the horizontal displacement field in the vertical direction. Areas darker or lighter than the background indicate discontinuities in the displacement field (i.e. discrete slip surfaces or faults). The plots are shown at 25, 50, 75, and 100% of the final fault slip.

(Sheory, 1994). It is therefore likely that the Rip Van Winkle anticline formed at high depths under high overburden loads. This is consistent with the thermal history of the rocks forming the anticline (Epstein et al., 1977; Friedman and Sanders, 1982; Lakatos and Miller, 1983).

Folding of the heterogeneous, layered sequence of La Zeta anticline cannot be explained by a model that uniformly dissipates the strain away from the fault, such as trishear. Rather, it is necessary to combine two modes of deformation: one converting faulting to folding up-section and the other transporting material from the backlimb into the hinge area in the less competent beds of the sequence.

The geometry of La Zeta anticline implies localized folding between units that behave brittlely (the Choiyoi Group and La Manga Formation, DEM simulations, Section 4). This type of deformation results from the combination of: (1) mechanical stratigraphy (i.e. the characteristic sedimentary sequence of La Zeta anticline), and (2) an initial state of stress characterized by a high K_o (high over-consolidation). We suggest that the anticline formed after substantial uplift of the Andean mountain front, under the high compressive horizontal stresses (high K_o) resulting from the Andean stress field and the gravitational instability created by the erosion of the mountain front and deposition of about 3 km of sediments in the adjacent foreland basin (Groeber, 1980).

Each of the techniques used in this paper has its advantages and limitations: kinematic models such as trishear conveniently reproduce the overall geometry and strain field of fault propagation folds in homogeneous sequences, yet the simplicity of the velocity field of the model is inadequate to capture processes typical of heterogeneous, layered sequences, such as backlimb layer parallel slip. Mechanical models such as the DEM are great tools to evaluate the effects of lithology, loading history (i.e. over-consolidation), and loading rates on fault propagation folding, yet the calibration and up-scaling of the models is not straightforward and their complexity makes them sometimes impractical. This paper shows that there is no unique mechanism of deformation (i.e. kinematics) that characterizes fault propagation folding. Fold kinematics is controlled by mechanical stratigraphy, initial state of stress, and fault-fold history (Jamison, 1992; Erslev and Mayborn, 1997). Only through the combination of detailed field studies, kinematic, and mechanical modeling will we be able to assess the effect of these variables.

Acknowledgements

We thank Maria Klemperer-Johnson, Ernesto Cristallini, José Silvestro, Tomás Zapata, Leandro Echavarría, and Andreas Kammer for assistance in the field and numerous constructive discussions. Rene Manceda from REPSOL-YPF generously shared his knowledge of the Malargüe–Bardas Blancas area. Ruben Zuñiga and family in Malargüe greatly facilitated logistics. DEM modeling was pursued at Rice University, The Norwegian Geotechnical Institute, and The Center for Integrated Petroleum Research. Eric Erslev generously provided us with his program LDIS, to construct

symmetric, smooth rose diagrams. Critical reviews by Eric Erslev and an anonymous reviewer improved the quality of the paper. This work was mainly supported by National Science Foundation grant EAR-0125557 to Richard Allmendinger. We also thank REPSOL-YPF, The Norwegian Research Council, and The Center for Integrated Petroleum Research for financial support.

References

Allmendinger, R.W., 1998. Inverse and forward numerical modeling of trishear fault-propagation folds. Tectonics 17 (4), 640–656.

Anderson, T.L., 1995. Fracture Mechanics, 2nd ed CRC Press, Boca Raton.

Chapman, T.J., Williams, G.D., 1985. Strains developed in the hanging walls of thrusts due to their slip/propagation rate, a dislocation model: reply. Journal of Structural Geology 7, 759–762.

Dessanti, R., 1973. Descripción geológica de la Hoja 29b, Bardas Blancas. Provincia de Mendoza. Servicio Nacional Minero Geológico, Boletín no. 139, Buenos Aires.

Dimieri, L.V., 1997. Tectonic wedge geometry at Bardas Blancas, southern Andes (36°S), Argentina. Journal of Structural Geology 19, 1419–1422.

Dominic, J.B., McConell, D.A., 1994. The influence of structural lithic units in fault related folds, Seminoe Mountains, Wyoming, USA. Journal of Structural Geology 16, 769–779.

Engelder, T., 1979. Mechanisms for strain within the Upper Devonian elastic sequence of the Appalachian Plateau, western New York. American Journal of Science 279, 527–542.

Engelder, T., Marshak, S., 1985. Disjunctive cleavage formed at shallow depths in sedimentary rocks. Journal of Structural Geology 7, 327–343.

Epstein, A.G., Epstein, J.B., Harris, L.D., 1977. Conodont color alteration—an index to organic metamorphism. U.S. Geological Survey Professional Paper 995.

Erickson, S.G., 1996. Influence of mechanical stratigraphy on folding vs. faulting. Journal of Structural Geology 18, 443–450.

Erslev, E.A., 1991. Trishear fault-propagation folding. Geology 19, 617–620.

Erslev, E.A., Mayborn, K.R., 1997. Multiple geometries and modes of fault propagation folding in the Canadian thrust belt. Journal of Structural Geology 19, 321–335.

Finch, E., Hardy, S., Gawthorpe, R., 2003. Discrete element modeling of contractional fault propagation folding above rigid basement blocks. Journal of Structural Geology 25, 515–528.

Fisher, D.M., Anastasio, D.J., 1994. Kinematic analysis of a large-scale leading edge fold, Lost River Range, Idaho. Journal of Structural Geology 16 (3), 337–354.

Friedman, G.M., Sanders, J.E., 1982. Time-temperature burial significance of Devonian anthracite implies former great (~6.5 km) depth of burial of Catskill Mountains, New York. Geology 10, 93–96.

Groeber, P., 1918. Estratigrafía del Dogger en La República Argentina, estudio sintético comparativo. Ministerio de Agricultura de la Nación, Dirección General de Minas, Geología e Hidrología, Boletín no. 18, Serie B, Buenos Aires.

Groeber, P., 1980. Observaciones geológicas a lo largo del meridiano 70. Asociación geológica Argentina, Serie C Reimpresiones 1.

Gulisano, C.A., Gutíerrez Pleimlig, A.R., 1994. The Jurassic of the Neuquén basin, field guide. Asociación Geológica Argentina, Serie E, no. 3. Secretaria de Minería de la Nación, Dirección Nacional del Servicio Geológico.

Harris, H.J., Van Der Pluijm, B.A., 1998. Relative timing of calcite twinning strain and fold-thrust belt development; Hudson Valley fold-thrust belt, New York, USA. Journal of Structural Geology 20, 21–32.

Ismat, Z., Mitra, G., 2001. Folding by cataclastic flow at shallow crustal levels in the Canyon Range, Sevier orogenic belt, west-central Utah. Journal of Structural Geology 23, 355–378.

Jamison, W.R., 1992. Stress controls on fold thrust style. In: McClay, K.R. (Ed.), Thrust Tectonics. Chapman and Hall, London, pp. 155–164.

King, G., Yielding, G., 1984. The evolution of a thrust fault system: processes of rupture initiation, propagation and termination in the 1980 El Asnam earthquake. Geophysical Journal of the Royal Astronomical Society 77, 915–933.

Lakatos, S., Miller, D.S., 1983. Fission-track analysis of apatite and zircon defines burial depth of 4–7 km for lowermost Upper Devonian Catskill Mountains, New York. Geology 11, 103–104.

Lambe, T.W., Withman, R.V., 1979. Soil Mechanics. John Wiley, New York.

Manceda, R., Figueroa, D., 1995. Inversion of the Mesozoic Neuquén rift in the Malargüe fold and thrust belt, Mendoza, Argentina. In: Tankard, A.J., Suárez, R., Welsink, H.J. (Eds.), Petroleum Basins of South America American Association of Petroleum Geologists Memoir, Tulsa, 62, pp. 369–382.

Manceda, R., Kozlowski, E., Cruz, C., Condat, P., 1990. Secuencia de techo pasiva estructurada, Bardas Blancas. Provincia de Mendoza, Argentina. 11th Congreso Geológico Argentino, Actas 2, pp. 31–34.

Manceda, R., Bolatti, E., Manoni, R., 1992. Modelo estructural para la zona de Bardas Blancas, Malargüe, provincia de Mendoza. Boletín de Informaciones Petroleras, Tercera Epoca 31, 92–103.

Marshak, S., 1986. Structure and tectonics of the Hudson Valley fold-thrust belt, eastern New York State. Geological Society of America Bulletin 97, 354–368.

Marshak, S., 1990. Structural geology of Silurian and Devonian strata in the Mid-Hudson Valley, New York: Fold-thrust belt tectonics in miniature. Geological Survey, New York State Museum, Map and Chart series number 41, Albany, New York.

Marshak, S., Engelder, T., 1985. Development of cleavage in limestones of a fold thrust belt in eastern New York. Journal of Structural Geology 7, 345–359.

Morgan, J.K., 1999. Numerical simulations of granular shear zones using the distinct element method: II. The effect of particle size distribution and interparticle friction on mechanical behavior. Journal of Geophysical Research B2, 2721–2732.

Morgan, J.K., 2004. Particle dynamics simulations of rate- and state-dependent frictional sliding of granular fault gouge. Pure and Applied Geophysics 161, 1877–1891.

Morgan, J.K., Boettcher, M.S., 1999. Numerical simulations of granular shear zones using the distinct element method. I. Shear zone kinematics and the micromechanics of localization. Journal of Geophysical Research B2, 2703–2719.

Morgan, J.K., McGovern, P.J., 2005. Discrete element simulations of gravitational volcanic deformation: 1. Deformation structures and geometries. Journal of Geophysical Research 110, B05402.

Ramos, V.A., Nullo, F.E., 1993. El volcanismo de Arco Cenozoico. In: Ramos, V.A. (Ed.), Geología y Recursos Naturales de Mendoza. 12th Congreso Geológico Argentino y 2nd Congreso Nacional de Exploración de Hidrocarburos. Relatorio, I(12), pp. 149–160.

Ramsay, J.G., Huber, M.I., 1987. The Techniques of Modern Structural Geology, Volume II: Folds and Fractures. Academic Press, London.

Sheory, P.R., 1994. A theory for in situ stresses in isotropic and transversely isotropic rock. International Journal of Rock Mechanics and Mining Sciences 31, 23–34.

Storti, F., Salvini, F., McClay, K., 1997. Fault related folding in sandbox analogue models of thrust wedges. Journal of Structural Geology 19, 583–602.

Strayer, L.M., Suppe, J., 2002. Out of plane motion of a thrust sheet during along-strike propagation of a thrust ramp: a distinct element approach. Journal of Structural Geology 24, 637–650.

Zehnder, A.T., Allmendinger, R.W., 2000. Velocity field for the trishear model. Journal of Structural Geology 22, 1009–1014.